UCPH NanoScience
NanoVidenskab KU

tidsskrift.dk/index.php/NanoVidenskabKU

Thesis Paper

Weyl semimetals in models for ultracold atoms

Andreas Hansen

Received June 2017, Accepted April 2018

I study the effect of a non-Abelian gauge potential on a Weyl semimetal phase appearing in a particular 3D tight-binding model of fermions. The lattice I consider is characterized by a C_3 rotational symmetry and by staggered $\pi/2$ magnetic fluxes on the triangular plaquettes in its horizontal planes. The energy spectrum is characterized by both single Weyl points with linear energy dispersions in all three momenta directions, and double Weyl points with quadratic energy dispersions in two directions and linear dispersion along the axis of the rotational symmetry.

1 Introduction

The study of topological phases of matter are at the focus of both theoretical and experimental studies. Most of the efforts have been devoted to the study of topological insulators and superconductors, which are gapped energy systems that can display non-local, topological features, which are robust against local noise and perturbations. The main robust features are usually related to the existence of gapless boundary states protected by the symmetries of the system [1]. These protections were believed to be based on the presence of an energy gap in the band structure but in the most recent years, it was proven that also gapless systems can display similar features. The simplest and first examples were Weyl semimetals [2], which are based on the massless fermions called Weyl fermions, that Hermann Weyl derived from the Dirac equation in 1929 [3].
The 3D Weyl semimetal contains zero-energy bulk modes with linear dispersion in all three momenta directions, called Weyl nodes, and their stability against perturbations gives rise to protected gapless surface modes called Fermi arcs [4]. The Weyl nodes also carry topological features corresponding to monopoles of the Berry flux.
Weyl semimetals are not the only possible semimetallic phase of matter with topological features as there are several proposals to create more exotic topological materials. Some of the proposals suggests topological materials characterized by multiple Weyl points, which have quadratic or even higher dispersion relations with multiple monopoles of the Berry flux [5].
The Weyl nodes were obtained in solid states systems by breaking the spatial inversion symmetry in several compounds such as tantalum arsenide [6–8] and niobium arsenide [9]. The appearance of gapless Fermi arcs have also been observed in tantalum arsenide through photoemission measurements [8]. Experimental realizations of Weyl nodes have also been found in photonic crystals with gyriod geomtry, where the inversion symmetry was broken by drilling holes with an additional element [10]. The breaking of time-reversal symmetry to obtain Weyl nodes has not been done experimentally but several proposals have been made [11,12].
The study of topological phases of matter is not only limited to solid state systems as the example of the photonic crystals showed. One of the other platforms to implement systems with topological features is with ultracold gases trapped in optical lattices and it gives an environment practically free from disorder, where the interactions among particles can be controlled with good accuracy. Recent experiments in the ultra cold atom platform demonstrated the possibility of engineering large magnetic fluxes, for example through laser-assisted tunneling [13,14] and spin-orbit couplings [15–17] .
In this paper I will make a proposal to obtain Weyl nodes with linear dispersions, called single Weyl points, and quadratic dispersions, called double Weyl points, in a 3D triangular lattice with $\pi/2$-flux and non-Abelian gauge potential. I will study a tight-binding model of two-component fermions with nearest-neighbor hoppings. In Section 2 I discuss the properties of a system with $\pi/2$-fluxes implemented by an Abelian gauge potential. In Section 3 I add a non-Abelian gauge potential, which resembles a spin-orbit coupling, to the system. In Section 4 I study and discuss the band structure and Weyl points (Section 4.1) and the symmetries of the system (Section 4.2). Finally, Section 5 is an overview of the possible future developments of the models, which include the analysis of its Fermi arcs and the experimental techniques to observe its band structures.

2 Triangular Lattice with staggered $\pi/2$-fluxes

Experiments have shown that it is possible to tune staggered magnetic fluxes in a triangular lattice with artificial gauge fields[18]. It is therefore reasonable to consider the theoretical analysis of a lattice model of fermions in a 3D stack of overlapping horizontal triangular lattices to get Weyl semimetals.
The x-y plane of the triangular lattice is shown in Figure 1. The lattice vectors $\vec{a}$ are given by:
$\vec{a}_1 = a\hat{x}$, $\vec{a}_2 = a\left(\frac{1}{2}\hat{x}+\frac{\sqrt{3}}{2}\hat{y}\right)$, $\vec{a}_3 = a\left(\frac{1}{2}\hat{x}-\frac{\sqrt{3}}{2}\hat{y}\right)$, $\vec{a}_4 = a\hat{z}$
where a is the lattice constant and $a = 1$ for simplicity.
The first Brillouin zone of the triangular lattice is defined by the reciprocal lattice vectors: $\vec{b}_1 = 2\pi\left(\hat{k}_x - \frac{1}{\sqrt{3}}\hat{k}_y\right)$, $\vec{b}_2 = \frac{4}{3}\sqrt{3}\,\hat{k}_y$, $\vec{b}_3 = 2\pi\left(\hat{k}_x + \frac{1}{\sqrt{3}}\hat{k}_y\right)$ and $\vec{b}_4 = 2\pi\hat{k}_z$.

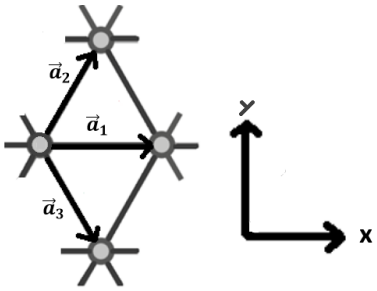

Fig. 1 The 2D x-y plane of the triangular lattice with hopping amplitudes t and lattice vectors a_1, a_2 and a_3 . The extension in the third direction, $\vec{a}_4$, is just an unitary vectors like $\vec{a}_1$.

I introduce an Abelian gauge potential $\vec{A}_{AB}$, which leads to induced fluxes with opposite sign for upwards and downwards pointing plaquettes in the triangular lattice[18] as shown in Figure 2. The flux in each plaquette is obtained through Stoke's theorem, which is the sum of the three hopping phases $\theta_j(\vec{r}) = \int_{\vec{r}}^{\vec{r}+\vec{a}_j} \vec{A}_{AB}(\vec{r}\,') \cdot d\vec{r}\,'$ equal to $\pm\pi/2$. The gauge choice does not have any physical consequences for the system, but the flux configuration shown in Figure 2 is gauge invariant property and defines the model.
The general tight-binding Hamiltonian for a system with phases is given as:

$$H = -t\sum_{\vec{r},\,j} e^{i\theta_j(\vec{r})}\, c^{\dagger}_{\vec{r}+\vec{a}_j} c_{\vec{r}} + h.c. \tag{2.1}$$

where $c^{\dagger}$ and c are creation and annihilation operators for fermions on the lattice, t is the hopping amplitude, $\theta_j(\vec{r})$ are the fluxes and $\vec{a}_j$ are the lattice vectors $\vec{a}_1$, $\vec{a}_2$, $\vec{a}_3$ and $\vec{a}_4$.

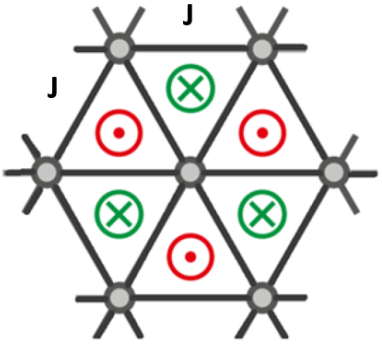

Fig. 2 Illustration inspired by J. Struck et al[18], which shows the gauge field applied to the triangular lattice system. The crosses correspond to inwards pointing gauge fluxes and dots correspond to outwards. The hopping amplitudes J are imaginary and the triangular lattice has the same lattice vectors $\vec{a}_j$ as in Figure 1.

I choose the specific configuration of $\pi/2$-fluxes for this model, so the triangular lattice gets imaginary hopping amplitude $J = i\,t$ and hopping vectors a_j as in Figure 1. The gauge choice gives the system $\pi/2$ phases in the x-y plane and z-direction and none of the vertical plaquettes have fluxes. The system has C_3 rotational symmetry around the z-axis, which will be discussed in Section 4.2.

3 Non-Abelian gauge potential as spin-orbit coupling

In the previous section I introduced staggered $\pi/2$ fluxes in the system, which only has a single band, and therefore not sufficient to give Weyl points. I expand the model with spin degree of freedom. In ultracold atom experiments the two spin species are usually given by hyperfine atomic species in current experiments[19,20]. Therefore to study the Weyl cones I introduce a spin 1/2 degree of freedom, whose dynamics is dictated by a non-Abelian gauge potential $\vec{A}_{NAB}$:

$$\vec{A}_{NAB} = q(\sigma_x, \sigma_y, \sigma_z) \tag{3.1}$$

where σ are Pauli matrices and the parameter q determines the intensity of the non-Abelian term $\vec{A}_{NAB}$[20]. The non-Abelian gauge potential couple, in general, the spin and the dynamics of the particles, like a spin-orbit coupling, which is different from the usual spin-orbit coupling like Rashba or Dresselhaus. The realization of this "3D Weyl spin-orbit coupling" has been proposed through suitable laser schemes in ultra-cold atoms[21,22] .
With the new gauge potential $\vec{A}$ consisting of $\vec{A}_{NAB}$ and $\vec{A}_{AB}$ the Hamiltonian can be written as:

$$H = -t\sum_{\vec{r},j,s,s'} U^{j}_{s,s'}\, c^{\dagger}_{\vec{r}+\vec{a}_j,s} c_{\vec{r},s'} + h.c. \tag{3.2}$$

where s and s' label the spin states. The unitary operators U are determined by the Abelian phases $e^{i\theta_j(\vec{r})}$, which match the ones in Section 2, and the non-Abelian component $\vec{A}_{NAB}$:

$$U^{j}_{s,\,s'} = e^{i\theta_j(\vec{r})} e^{i\int_{\vec{r}}^{\vec{r}+\vec{a}_j} \vec{A}_{NAB}(\vec{r}\,')\cdot d\vec{r}\,'} \tag{3.3}$$

I consider the unitary operators in Equation 3.3, which are the tunneling operators in the system, consisting of the staggered Abelian $\pi/2$ fluxes from Section 2 and the non-Abelian "Weyl" spin-orbit coupling given by Equation 3.1. The tunneling operators are:

$$\begin{aligned} U_1 = i\,e^{iq\sigma_x}\ ,\ U_2 = i\,e^{iq\left(\frac{1}{2}\sigma_x+\frac{\sqrt{3}}{2}\sigma_y\right)}\ , \\ U_3 = i\,e^{iq\left(\frac{1}{2}\sigma_x-\frac{\sqrt{3}}{2}\sigma_y\right)}\ ,\ U_4 = i\,e^{iq\sigma_z} \end{aligned} \tag{3.4}$$

With the tunneling operators in Equation 3.4 the Hamiltonian for the system in momentum space $H(\vec{k})$ is written in the Weyl Hamiltonian form:

$$H(\vec{k}) = \alpha_0(\vec{k})\sigma_0 + \alpha_x(\vec{k})\sigma_x + \alpha_y(\vec{k})\sigma_y + \alpha_z(\vec{k})\sigma_z \tag{3.5}$$

where σ_0 is the 2x2 identity matrix and the momentum coefficients are given as :

$$\alpha_0 = 2t\cos(q)\left(\sin(k_x) + 2\sin\left(\frac{k_x}{2}\right)\cos\left(\frac{\sqrt{3}k_y}{2}\right) + \sin(k_z)\right) \tag{3.6}$$

$$\alpha_x = 2t\sin(q)\left(\cos(k_x) + \cos\left(\frac{k_x}{2}\right)\cos\left(\frac{\sqrt{3}k_y}{2}\right)\right) \tag{3.7}$$

$$\alpha_y = -2\sqrt{3}\,t\ \sin(q)\left(\sin\left(\frac{k_x}{2}\right)\sin\left(\frac{\sqrt{3}k_y}{2}\right)\right) \tag{3.8}$$

$$\alpha_z = 2t\sin(q)\cos(k_z) \tag{3.9}$$

When the Hamiltonian in Equation 3.5 is diagonalized the energy is given by:

$$E(\vec{k}) = \alpha_0(\vec{k}) \pm \sqrt{\left(\alpha_x(\vec{k})\right)^2 + \left(\alpha_y(\vec{k})\right)^2 + \left(\alpha_z(\vec{k})\right)^2} \tag{3.10}$$

When the $q = 0$ the energy E in Equation 3.10 reduces to α_0 which is equivalent to Equation 3.6, and it matches the spectrum of the $\pi/2$-flux model from Section 2, and the Hamiltonian H in Equation 3.5 also reduces to this model. The parameter q is limited to $0 \leq q < \pi$ because of the relation $H(q) = -H(q+\pi)$.
The spectrum of the Hamiltonian in Equation 3.5 is characterized by both Weyl points and double Weyl points, and the the properties of the points and symmetries of the Hamiltonian will be discussed in Section 4 based on the works of Reference 5.

4 Weyl points of the system

4.1 Band structure and Weyl points

The single Weyl points have a linear energy dispersions along the three momenta directions and have a topological charge, which is associated with Berry flux of $2\pi\kappa$ where $\kappa = \pm 1$ is the chirality[23]. The double Weyl points are quadratic along two directions and linear in the third and carry a double monopole of the Berry flux, which is behaving topologically as two Weyl points with the same charge.
In order to identify and describe the Weyl points properly we first look at the band touching points of the first Brillouin zone. The energy spectrum of Equation 3.10 gives band touching points for any value of $q \neq 0$ at $\pi\left(0, \frac{2}{\sqrt{3}}, \pm\frac{1}{2}\right)$, $\pi\left(\pm\frac{2}{3}, 0, \pm\frac{1}{2}\right)$, $\pi\left(\pm\frac{2}{3}, \frac{4}{\sqrt{3}}, \pm\frac{1}{2}\right)$, $\pi\left(\pm\frac{4}{3}, \pm\frac{2}{\sqrt{3}}, \pm\frac{1}{2}\right)$, which corresponds to four inequivalent Weyl points and two double Weyl points in the first Brillouin zone. The band touching points can be studied if one consider the gap between the valence (lowest) and conduction (highest) band, given by $\Delta E = 2\sqrt{\alpha_x^2 + \alpha_y^2 + \alpha_z^2}$, in the first Brillioun zone for one of the momenta planes (k_x-$\tilde{k}_y$ plane). The shifted momentum $\tilde{k}_y$ is a gauge transformation, $\tilde{k}_y = k_y - \frac{2\pi}{\sqrt{3}}$, and the k_x-$\tilde{k}_y$ plane is shown in Figure 3.

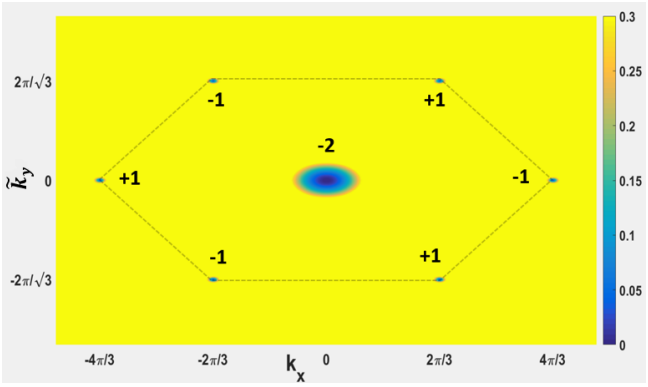

Fig. 3 Energy gap between the valence and conduction band in one of the k_x-$\tilde{k}_y$ planes ($k_z = +\pi/2$) where the band touching points are shown with their corresponding topological charge. The momenta direction k_y is shifted as $\tilde{k}_y = k_y - \frac{2\pi}{\sqrt{3}}$. There are two inequivalent Weyl points with ± 1 charge at the corners of the first Brillouin zone (shown as black dotted hexagon) and one double Weyl point with -2 charge at the middle of the 2D projection of the Brillouin zone.

The band touching points corresponds, as mentioned earlier, to two inequivalent Weyl points with topological charges ± 1 and one double Weyl point with topological charge $+2$ in the plane shown in Figure 3 and opposite topological charges for the k_x-$\tilde{k}_y$ plane with $k_z = -\pi/2$.

In this 2D Brillioun Zone all the single Weyl points are on the corners of the first Brillioun zone, and the double Weyl point is in the center. An important requirement to satisfy in regards to the topological charge is the Nielsen-Ninomiya theorem[24] which states that the sum of the topological charge for all the Weyl points (single and double) must be 0. This is also true for this system since all the Weyl points comes in pair in the first Brillouin zone.

The filling of the bands, and how the parameter q, in the spin-orbit term, changes the energy of the bands, will be discussed in the following. I will first consider $q = \pi/2$, resulting in $\alpha_0 = 0$, and then how the system evolves for q different from $q = \pi/2$.
I plot the energy in the k_x-$\tilde{k}_z$ plane ($k_y = 0$) with $q = \pi/2$, where the shifted momentum is $\tilde{k}_z = k_z - \frac{\pi}{2}$, in Figure 4, which shows three Weyl points. Two of the Weyl points are single Weyl points in which the energy dispersions are linear in all momenta directions, and for the double Weyl point the energy dispersion is quadratic in the k_x-k_y plane and linear in k_z.

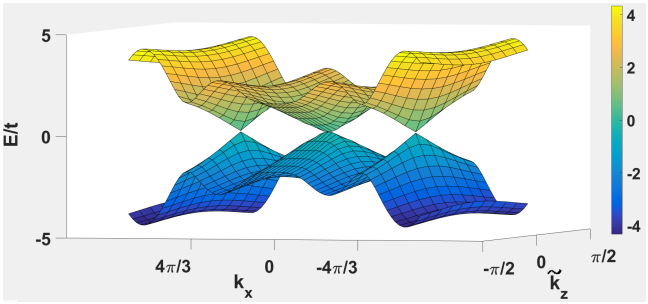

Fig. 4 The energy dispersion with $q = \frac{\pi}{2}$ for the k_x-$\tilde{k}_z$ plane is shown for $k_y = 0$. The momentum is shifted as $\tilde{k}_z = k_z - \frac{\pi}{2}$. Two inequivalent Weyl points with different charges ± 1 with linear dispersions in the k_x-$\tilde{k}_z$ plane are shown. The double Weyl point has quadratic dispersion in k_x-direction and in k_z-direction it has linear dispersion.

The Weyl points all have zero energy at $q = \pi/2$, which means the Fermi surface at half filling includes only discrete points, and therefore both the bands are partially filled.
In the case of $q \neq \pi/2$ the bands start to overlap in energy as shown in Figure 5, where $q = 2\pi/5$. In the Brillouin zone two single Weyl points with different charges have the highest energy and two Weyl points with opposite charges at the lowest energy.
The energy value of the double Weyl points is still 0 as in the case for $q = \pi/2$ thus it does not depend on the parameter q and the filling of the double Weyl with fermions can be expressed as $N_E = L^3$, where L is length of one of the dimensions of the system.

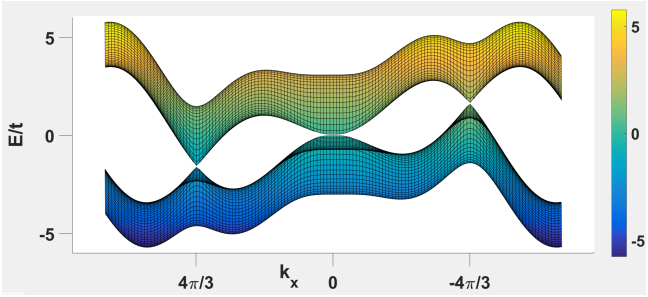

Fig. 5 An example of one the k_x-$\tilde{k}_z$ planes ($k_y = 0$). The energy dispersion with $q = \frac{2\pi}{5}$ for the k_x-$\tilde{k}_z$ plane is shown for $k_y = 0$. Only the k_x direction is shown in this Figure for better clarity of the energy values. In this plane the single Weyl point with negative topological charge has negative energy and positive charge has positive energy.

4.2 Symmetries of the system

The single Weyl points are protected by their topological charge and they can only be destroyed by coupling a pair of Weyl points with opposite charges. This means that, if they lie in different positions in momentum space, it is not possible to open a gap with weak perturbations, unless these perturbations break translational invariance. The single Weyl points are protected by translational invariance and local and uniform perturbations can not destroy the single Weyl points.
I will consider the effect of local and uniform perturbations on the double Weyl points and consider what symmetries are protecting them. A double Weyl points can be split in general into two equal Weyl points by local perturbations. I consider the generic effect of a local, translational invariant perturbation P on the Hamiltonian:

$$H = H_0 + P \tag{4.1}$$

where H_0 is the non-perturbed Hamiltonian. The perturbation P is a local and position independent operator and I will only consider the perturbations which do not break the single Weyl points, since that double Weyl points are more fragile than the single Weyl points. The perturbation consists of Zeeman terms $(\sigma_x, \sigma_y, \sigma_z)$, where σ_z does not break the rotational symmetry of the system, since it is along the z-axis, and will shift the double Weyl points along the z-axis. The other Zeeman terms, σ_x and σ_y, do break the rotational symmetry and destroy the double Weyl points, which is consistent with the results of Reference 5. A study has shown C_6-symmetry can protect the double Weyl point[5] and another study shows C_3 with time-reversal symmetry also protects the double Weyl[25].
The system described by Section 4 has C_3-symmetry (shown in Appendix D) and particle-hole symmetry (shown in Appendix E), which is reminiscent of the C_3 with time-reversal symmetry.

To analyze the band touching points in this model, I expand the Hamiltonian close to a double Weyl and translate the momenta k_y and k_z and consider the Taylor expansions on an effective low-energy level and get the effective Hamiltonian H_{eff}. The band structure of the model close to the double Weyl points, with the shifted momenta $\tilde{k}_y$ and $\tilde{k}_z$ can be described by:

$$H_{eff}(\vec{k}) = \left(-\frac{3}{4}\, t\ sin(q)\ k_x^2 + \frac{3}{4}\, t\ sin(q)\ \widetilde{k}_y^{\,2}\right)\sigma_x + \left(\frac{3}{2}\, t\ sin(q)\ k_x\, \widetilde{k}_y\right)\sigma_y - 2\, t\ sin(q)\ \widetilde{k}_z\ \sigma_z \tag{4.2}$$

The effective Hamiltonian H_{eff} is invariant under C_6-symmetry and therefore the energy bands of H_{eff} are eigenvalues of C_6. I label u_c and u_v the eigenvalues of the conductance and valence bands under a $\pi/3$ rotation. When u_c and u_v are different from each other $\langle\psi_1|P|\psi_2\rangle = 0$ unless the perturbation P is not invariant under C_6-symmetry .
If P does not depend momentum or position the gap cannot open unless it violates the C_6-symmetry and so it must be that the double Weyl points are protected from any perturbation which does not violate the rotational symmetry.

5 Further developments of the model

As seen in Figure 3 the band touching points with the same k_x and k_z coordinates have the same topological charge. This suggests than when they are projected in the k_y directions opposite topological charges do not overlap. Therefore Fermi arcs appear on surfaces at fixed y. It could be possible to explore the Fermi arcs if a hard-wall potential is confining the potential and gives the system a finite size in the y-direction ($y = 0, ..., L$) [4]. The detailed analysis of the wavefunctions and properties of the Fermi arcs of the confined system are beyond the scope of this work and may be subject of further investigations.
A proposal for the detection of the band touching points experimentally is the Landau Zener experiments[26,27], which looks at the transitions of some of the fermions from the lower band to the upper band. It may be possible to detect how many fermions are in the upper band by time of flight measurements and ideally distinguish between the single and double Weyl points . If the Landau Zener experiments becomes able to detect band touching points and Weyl points, it could be an interesting way to study the model presented in this paper experimentally.

6 Conclusions

I analyzed a tight-binding model of fermions hopping in a 3D lattice and subjected it to a gauge potential and I introduced staggered $\pi/2$ fluxes on the triangular plaquettes with an Abelian gauge potential. To study Weyl points I expanded the model with spin degree of freedom and introduced a spin 1/2 degree of freedom, whose dynamics was dictated by a non-Abelian gauge potential. The non-Abelian gauge coupled the spin and the dynamics of the particles like a spin-orbit coupling.
The band structure was characterized by four single Weyl points at the corners of the first Brillouin zone and two double Weyl points in the center of the k_x-k_y planes, which had topological charges. The energy of the single Weyl points were depend on the spin-orbit intensity but the double Weyl points were at 0 energy at any intensity.
The symmetries protecting the double Weyl points were explored as the system contained C_3 rotational symmetry and particle hole symmetry. At a low-energy level the system had C_6 symmetry, which can protect the double Weyl points from any pertubation, which does not violate the rotational symmetry. I finally suggested possible further developments of the model, which included the study of Fermi arcs of the system and the detection of Weyl points through Landau Zener experiments.

7 Acknowledgements

I would like to thank my supervisor Michele Burrello for the inspiration to this project, and for helping whenever a problem occurred. It has been a good introduction into the realm of condensed matter theory, ultracold atoms and Weyl semimetals.

References

1 M. Z. Hasan and C. L. Kane, *Rev. Mod. Phys.*, 2010, **82**, 3045–3067.
2 F. C. Yan, B., *Annual Review of Condensed Matter Physics*, 2017, **8**, 337–354.
3 H. Weyl, *Zeitschrift fur Physik*, 1929, **56**, 330–352.
4 X. Wan, A. M. Turner, A. Vishwanath and S. Y. Savrasov, *Phys. Rev. B*, 2011, **83**, 205101.
5 C. Fang, M. J. Gilbert, X. Dai and B. A. Bernevig, *Phys. Rev. Lett.*, 2012, **108**, 266802.
6 B. Q. Lv and et al., *Nature Physics*, 2015, **11**, 724–727.
7 B. Q. Lv and et al., *Phys. Rev. X*, 2015, **5**, 031013.
8 M. Z. Hasan, S.-Y. Xu and et al., *Science*, 2015, **349**, 613–617.
9 M. Z. Hasan, S.-Y. Xu and et al., *Nat Phys*, 2015, **11**, 748–754.
10 L. Lu, Z. Wang, D. Ye, L. Ran, L. Fu, J. D. Joannopoulos and M. Soljačić, *Science*, 2015, **349**, 622–624.
11 A. A. Burkov and L. Balents, *Phys. Rev. Lett.*, 2011, **107**, 127205.
12 S. Ganeshan and S. D. Sarma, *Physical Review B*, 2015, **91**, 125438.
13 M. Aidelsburger, M. Atala, M. Lohse, J. T. Barreiro, B. Paredes and I. Bloch, *Physical Review Letters*, 2013, **111**, 185301.
14 H. Miyake, G. A. Siviloglou, C. J. Kennedy, W. C. Burton and W. Ketterle, *Physical Review Letters*, 2013, **111**, 185302.
15 B. M. Anderson, G. Juzeliūnas, V. M. Galitski and I. B. Spielman, *Physical Review Letters*, 2012, **108**, 235301.
16 B. Yadin and V. Vedral, *Phys. Rev. A*, 2016, **93**, 022122.
17 J. Armaitis, J. Ruseckas and G. Juzeliūnas, *Phys. Rev. A*, 2017, **95**, 033635.

18 J. Struck, M. Weinberg, C. Ölschläger, P. Windpassinger, J. Simonet, K. Sengstock, R. Höppner, P. Hauke, A. Eckardt, M. Lewenstein and L. Mathey, *Nature Physics*, 2013, **9**, 738–743.
19 J. Dalibard, F. Gerbier, G. Juzeliūnas and P. Öhberg, *Reviews of Modern Physics*, 2011, **83**, 1523–1543.
20 N. Goldman, G. Juzeliūnas, P. Öhberg and I. B. Spielman, *Reports on Progress in Physics*, 2014, **77**, 126401.
21 J. Armaitis, J. Ruseckas and G. Juzeliūnas, *Phys. Rev. A*, 2017, **95**, 033635.
22 J. P. Vyasanakere, S. Zhang and V. B. Shenoy, *Phys. Rev. B*, 2011, **84**, 014512.
23 A. M. Turner and A. Vishwanath, *ArXiv e-prints*, 2013.
24 H. B. Nielsen and M. Ninomiya, *Phys. Lett.*, 1981, **B105**, 219–223.
25 W.-J. Chen, M. Xiao and C. T. Chan, *Nature Communications*, 2016, **7**, 13038.
26 L. Tarruell, D. Greif, T. Uehlinger, G. Jotzu and T. Esslinger, *Nature*, 2012, **483**, 302–305.
27 W.-Y. He, S. Zhang and K. T. Law, *Phys. Rev. A*, 2016, **94**, 013606.
28 N. Goldman, G. Juzeliūnas, P. Öhberg and I. B. Spielman, *Reports on Progress in Physics*, 2014, **77**, 126401.
29 E. Matsuoka, K. Hayashi, A. Ikeda, K. Tanaka, T. Takabatake and M. Matsumura, *Journal of the Physical Society of Japan*, 2005, **74**, 1382–1385.

A Appendix: Second Quantization

Second quantization is the standard formulation of quantum many-particle theory. I will consider a free non-relativistic in a box with indistinguishable particles, which are translation invariant. This means the single particle wavefunctions are plane waves and for fermions we need to also consider the spin, so the single particle wavefunctions are given by:

$$\psi_{\vec{k},s} = \frac{1}{\sqrt{V}} e^{i\,\vec{k}\cdot\vec{r}}\sigma_s \tag{A.1}$$

where s is a spin index of either spin up or spin down. We would like to label the basis states in Fock space with occupation numbers $\{n_k\} = \{n_1, n_2, ...\}$ We now introduce the creation operator $c^\dagger_{\vec{k}}$ acting on some state in our Fock space, which adds a particle to the system. The Hermitian conjugate of the creation operator is the annihilation operator $c_{\vec{k}}$, which removes (or annihilates) a particle from the system. By definition the annihilation operator acting on a vacuum state $|0\rangle$ with no particles is given as:

$$c_{\vec{k}}\,|0\rangle = 0 \tag{A.2}$$

In the case of fermions the creation $c^\dagger_{\vec{k}}$ and annihilation operators $c_{\vec{k}}$ have anti-commutation relations since the wavefunction is antisymmetric:

$$\{c_{\vec{k}}, c^\dagger_{\vec{k}'}\} = \delta_{k,k'} \tag{A.3}$$

$$\{c_{\vec{k}}, c_{\vec{k}'}\} = \{c^\dagger_{\vec{k}}, c^\dagger_{\vec{k}'}\} = 0 \tag{A.4}$$

The single particle momentum state $|k\rangle$ can be expressed as:

$$c^\dagger_{\vec{k}}\,|0\rangle = |\vec{k}\rangle \tag{A.5}$$

which is the creation operator $c^\dagger_{\vec{k}}$ acting on the vaccum state $|0\rangle$.
The single particle in a box has a wavefunction, which can be expressed at the integral over the box:

$$|\vec{k}\rangle = \frac{1}{\sqrt{V}} \int d^3\vec{r}\; e^{i\,\vec{k}\cdot\vec{r}}\,|\vec{r}\rangle \tag{A.6}$$

and the inverse relation with real space wavefunction:

$$|\vec{r}\rangle = \frac{1}{\sqrt{V}} \sum_{\vec{k}} e^{-i\,\vec{k}\cdot\vec{r}}\,|k\rangle \tag{A.7}$$

It is required that the real space creation operator $|\vec{r}\rangle$ satisfies:

$$c^\dagger_{\vec{r}}\,|0\rangle = |\vec{r}\rangle \tag{A.8}$$

The relations between the creation annihilation and creation creation operators in momentum space and real space can be defined by the use of Equations A.5, A.6 and A.8. given as:

$$c_{\vec{k}} = \frac{1}{\sqrt{V}} \sum_{\vec{r}} e^{i\,\vec{k}\cdot\vec{r}} c_{\vec{r}} \tag{A.9}$$

and the inverse Fourier transform:

$$c_{\vec{r}} = \frac{1}{\sqrt{V}} \sum_{\vec{k}} e^{-i\,\vec{k}\cdot\vec{r}} c_{\vec{k}} \tag{A.10}$$

We can proof the transformation and inverse transformation:

$$c_{\vec{r}} = \frac{1}{\sqrt{V}} \sum_{\vec{k}} e^{-i\,\vec{k}\cdot\vec{r}} c_{\vec{k}} = \frac{1}{\sqrt{V}} \sum_{\vec{k}} e^{-i\,\vec{k}\cdot\vec{r}} \sum_{\vec{r}\,'} e^{i\,\vec{k}\cdot\vec{r}\,'}\, c_{\vec{r}\,'} = \sum_{\vec{r}\,'} c_{\vec{r}\,'} \frac{1}{\sqrt{V}} \sum_{\vec{k}} e^{-i\,\vec{k}(\vec{r}-\vec{r}\,')} = \sum_{\vec{r}\,'} c_{\vec{r}\,'}\,\delta_{\vec{r}\,\vec{r}\,'} = c_{\vec{r}} \tag{A.11}$$

An example of how to Fourier transform the sums from real space to momentum space is shown for a 1D chain given the sum $\sum_r c^\dagger_{r+1}\, c_r$:

$$\sum_r c^\dagger_{r+1}\, c_r = \sum_r \frac{1}{\sqrt{L}} \sum_k e^{i\,k(r+1)} c^\dagger_k \frac{1}{\sqrt{L}} \sum_{k'} e^{-i\,k'r} c_{k'} = \frac{1}{L} \sum_r \sum_{k,k'} e^{i\,k(r+1)} e^{-i\,k'r} c^\dagger_k c_{k'} \tag{A.12}$$

and using $e^{i\,k(r+1)} e^{-i\,k'r} = e^{i(k-k')\,r+i\,k}$ and seperating them:

$$\frac{1}{L} \sum_r \sum_{k,k'} e^{i\,k(r+1)} e^{-i\,k'r} c^\dagger_k c_{k'} = \sum_{k,k'} c^\dagger_k c_{k'}\; e^{i\,k} \frac{1}{L} \sum_r e^{i\,(k-k')\,r} = \sum_{k,k'} c^\dagger_k c_{k'}\; e^{i\,k}\; \delta_{k\,k'} = \sum_k c^\dagger_k c_k\; e^{i\,k} \tag{A.13}$$

The transformation is for the 1D case:

$$\sum_r c^\dagger_{r+1}\, c_r = \sum_k c^\dagger_k c_k\; e^{i\,k} \tag{A.14}$$

and for the Hermitian conjugated:

$$\sum_r c^\dagger_r\, c_{r+1} = \sum_k c^\dagger_k c_k\; e^{-i\,k} \tag{A.15}$$

B Appendix: Gauge Transformations

I will review some basic concept about gauge transformations in quantum systems and for simplicity consider the case of a wavefunction in free space. However the following definitions can be generalized to the lattice case relevant for ultracold atoms trapped in optical lattices. [28].

B.1 Abelian gauge transformation

The Abelian gauge transformation is a local transformation and, if we describe a dynamical system, depended on the space-time coordinates , with a complex function $\psi(x)$, we can express the Abelian gauge transformation as:

$$\psi(x) \rightarrow \psi'(x) = U(x)\psi(x) \tag{B.1}$$

where $U(x) = e^{i\theta(x)}$ is a unitary operator and belongs in the unitary group $U(1)$ and it depends on the position in $\theta(x)$. When a particle follows a path from a reference point j to a point k. It acquires a "magnetic phase factor" [28]:

$$\psi(\vec{r}_k) = exp\left(\frac{i}{\hbar}\int_j^k A(x)\cdot d\vec{l}\right)\psi_0(\vec{r}_k) = U_{jk}\psi_0(\vec{r}_k) \tag{B.2}$$

where $\psi_0(\vec{r}_k)$ is the wavefunction in the absence of the gauge potential and $U_{jk} = e^{i\phi_{jk}}$ is the tunneling operator.
In the case of an Abelian gauge transformation a particle subjected to a local gauge potential $A(x)$ and the non-relativistic single-particle Hamiltonian reads:

$$H = \frac{(p+A(x))^2}{2m} \tag{B.3}$$

where $p = -i\partial x$ and with the phase difference term $U(x)$ we can calculate that:

$$H = \frac{U^\dagger(p+A(x))^2U}{2m} \rightarrow \frac{(-i\partial x + \partial x\theta(x) + A(x))^2}{2m} \tag{B.4}$$

where the gauge potential $A(x)$ for the Abelian gauge transformation is transformed as:

$$A(x) \rightarrow A'(x) + \partial x\theta(x) = A(x) + U^\dagger(-i\,\partial x\,U) \tag{B.5}$$

The tunneling operators transforms as:

$$U_{jk} \rightarrow U'_{jk} = U_{jk}\,exp\left(i\,\frac{\theta(\vec{r}_k) - \theta(\vec{r}_j)}{\hbar}\right) \tag{B.6}$$

The following is a inclusion of lattice models. We will consider a square lattice in the explanation of plaquettes. The plaquettes, a closed region in space delimited by a set of points, are connected by links as shown in Figure B.1:

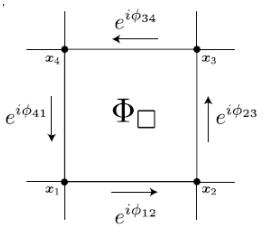

Fig. B.1 Figure from Ref. 28 showing the plaquette, tunneling operators and magnetic flux.

When the particle performs a loop $\square$ around the plaquette it gains an Aharonov-Bohm phase:

$$\psi(\vec{r}_1) \rightarrow \frac{i}{\hbar}\oint_\square A(x)\cdot d\vec{l}\,\psi(\vec{r}_1) = e^{2\pi i\Phi_\square}\psi(\vec{r}_1) \tag{B.7}$$

where $\Phi_\square$ is the number of magnetic flux quanta Φ_0 penetrating the plaquette $\square$ and it is expressed with the "loop product"t of tunneling operators U_{jk}:

$$e^{2\pi i\Phi_\square} = U_{12}\,U_{23}\,U_{34}...U_{L-1}\,U_{L1} = \prod_\square U_{jk} = exp\left(i\sum_\square \phi_{jk}\right) \tag{B.8}$$

In order to describe a lattice of a quantum system subject to a gauge potential the gauge potential A the lattice description should include:

1. A set of lattice sites $\vec{r}_j$
2. A set of links, j to k, connecting the sites and defining plaquettes
3. A set of tunneling operators U_{jk} associated with the links

B.2 Non-Abelian gauge transformation

If the tunneling operators U_{jk} couple to internal degrees of freedom, like the spin, gauge potentials act differently on the different spin states, and they are now matrix-valued objects. Tunneling operators now belong to the $SU(2)$ group and the potential $\vec{A}$ is a vector of matrices $\vec{A} = q(\sigma_x, \sigma_y, \sigma_z)$
The tunneling operator U_{jk} is given now dependent on the link j to k and the different spin states s and s' :

$$U_{jk,s,s'} = P \exp\left(\frac{i}{\hbar}\int_j^k \vec{A}_{s,s'} \cdot d\vec{l}\right) \tag{B.9}$$

where P is a path ordered integral and is required because at at different points of the path the matrices $\hat{A}_{z,y}$ do not necessarily commute.
In the case of the non-Abelian gauge transformations we must distinguish between global and local gauge transformations.

Global non-Abelian gauge transformation:
The global non-Abelian gauge transformation is given by

$$\psi \to \psi' = U\psi \tag{B.10}$$

where the unitary operator $U = e^{i\vec{\alpha}\vec{\sigma}}$ is not position dependent and it belongs to the $SU(2)$ unitary group.
The Hamiltonian for a system subjected to a global non-Abelian gauge transformation is

$$H = \frac{(\vec{p}\,\sigma_0 + \vec{A})^2}{2m} \to \frac{U^\dagger(\vec{p}\,\sigma_0 + \vec{A})^2 U}{2m} \tag{B.11}$$

and through calculations the global non-Abelian gauge potential can be described as

$$\vec{A} \to \vec{A}' = U^\dagger \vec{A}\, U \tag{B.12}$$

Local non-Abelian gauge transformation:
The local non-Abelian gauge transformation is given by:

$$\psi(x) \to \psi'(x) = U(x)\psi(x) \tag{B.13}$$

where the unitary operator $U = e^{i\vec{\alpha}(x)\vec{\sigma}}$ is position depend and it belongs to the $SU(2)$ unitary group.
The Hamiltonian for a system subjected to a local non-Abelian gauge transformation is:

$$H = \frac{(\vec{p}\,\sigma_0 + \vec{A}(x))^2}{2m} \to \frac{U^\dagger(x)(\vec{p}\,\sigma_0 + \vec{A}(x))^2 U(x)}{2m} \tag{B.14}$$

and through calculations the local non-Abelian gauge potential can be described as:

$$\vec{A}(x) \to \vec{A}(x)' = U^\dagger \vec{A}(x) U + \partial x \vec{\alpha}(x) \cdot \vec{\sigma} \tag{B.15}$$

C Appendix: Calculation of Berry Monopoles

I will briefly review how to calculate the Chern number of a touching point, which corresponds to the topological charge of a Berry monopole. Given the Hamiltonian $H(\vec{k}) = -\vec{k}\cdot\vec{\sigma}$, where $\vec{\sigma}$ is the Pauli matrix, we consider the states $|\uparrow\rangle$ and $|\downarrow\rangle$ and label the states α and β.
If we consider the Bloch sphere in Figure C.1 we can describe the wave function of a band by spherical coordinates.

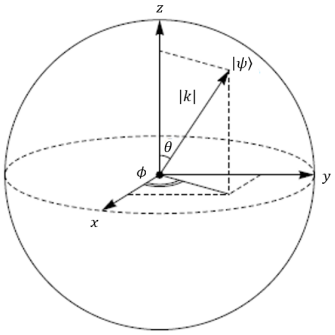

Fig. C.1 The Bloch sphere with the spherical coordinates ϕ, θ and k.

I consider the example with the state $|\psi\rangle$ given by Equation C.1

$$|\psi\rangle = \begin{pmatrix} \alpha = \cos(\frac{\theta}{2}) \\ \beta = e^{i\,\phi}\sin(\frac{\theta}{2}) \end{pmatrix} \tag{C.1}$$

Then we calculate the Berry connection $A(\vec{k})$, which is similar to a vector potential in momentum space and is given by Equation C.2

$$A(\vec{k}) = i\,\langle\psi(\vec{k})|\vec{\nabla}_k\psi(\vec{k})\rangle \tag{C.2}$$

If $\vec{\nabla}_k$ is written in spherical coordinates, as shown in Equation C.3, we can calculate the Berry connection in Equation C.2.

$$\vec{\nabla}_k = \left(\partial k, \frac{1}{k}\partial\theta, \frac{1}{k\,\sin(\theta)}\partial\phi\right) \tag{C.3}$$

The three spherical components of the Berry connection is calculated in Equation C.4-C.6

$$A_k(\vec{k}) = 0 \tag{C.4}$$

$$A_\theta(\vec{k}) = \frac{1}{k}\left(-\frac{1}{2}\cos\left(\frac{\theta}{2}\right)\sin\left(\frac{\theta}{2}\right) + \frac{1}{2}\cos\left(\frac{\theta}{2}\right)\sin\left(\frac{\theta}{2}\right)\right) = 0 \tag{C.5}$$

$$A_\phi(\vec{k}) = -\frac{1}{k\sin(\theta)}\left(\sin^2\left(\frac{\theta}{2}\right)\right) \neq 0 \tag{C.6}$$

The Berry connection in the ϕ direction (Equation C.6) is the only term not equal to 0.
We can use the Berry connection as a vector potential in regards to calculate the magnetic field given as C.7

$$\vec{F} = \vec{\nabla}\times\vec{A} \tag{C.7}$$

where the curl $\vec{\nabla}\times\vec{A}$ in spherical coordinates is given as C.8

$$\vec{F} = \vec{\nabla}\times\vec{A} = \frac{1}{k\sin(\theta)}\left(\frac{\partial}{\partial\theta}(A_\phi sin(\theta)) - \frac{\partial A_\theta}{\partial\phi}\right)\hat{k} + \frac{1}{k}\left(\frac{1}{sin(\theta)}\frac{\partial A_k}{\partial\phi} - \frac{\partial}{\partial k}(kA_\phi)\right)\hat{\theta} + \frac{1}{k}\left(\frac{\partial}{\partial k}(kA_\theta) - \frac{\partial A_k}{\partial\theta}\right)\hat{\phi} \tag{C.8}$$

We can reduce Equation C.7 by using the results of the Berry connections in Equations C.4-C.6 as shown in Equation C.9-C.11

$$F_k = \frac{1}{k\sin(\theta)}\left(\frac{\partial}{\partial\theta}(A_\phi sin(\theta))\right) = -\frac{1}{2k^2} \tag{C.9}$$

$$F_\theta = \frac{1}{k}\left(-\frac{\partial}{\partial k}(kA_\phi)\right) = \frac{1}{k}\frac{\partial}{\partial k}\left(\frac{1}{\sin(\theta)}\,\sin^2\left(\frac{\theta}{2}\right)\right) = 0 \tag{C.10}$$

$$F_\phi = \frac{1}{k}\left(\frac{\partial}{\partial k}(kA_\theta) - \frac{\partial A_k}{\partial\theta}\right) = 0 \tag{C.11}$$

Since we have fluxes from a sphere the only direction we consider is the k direction, which goes outward of the sphere, so the surface I consider is a oriented surface. The Chern number c_n can be calculated as the surface integral of magnetic fluxes given in Equation C.12 [29]

$$c_n = \frac{1}{2\pi}\int d^2k\;\hat{k}\cdot\vec{F} = \frac{1}{2\pi}\int d^2k\;F_k \tag{C.12}$$

The integral is the area of the Bloch sphere and the Chern number becomes:

$$c_n = \frac{1}{2k^2}(4\pi k^2)\left(-\frac{1}{k^2}\right) = -1 \tag{C.13}$$

The Chern number -1 corresponds to a Berry monopole with topological charge of -1.
If one considers different wave functions of a band $|\psi\rangle$ the topological charges may change to be ± 1.

D Calculation of the C_3 rotation symmetry

To show the C_3 rotation symmetry we need to satisfy the following:

$$\tilde{H}_0(R\vec{k}) = C_3^{\dagger}\tilde{H}_0 C_3 \tag{D.1}$$

where R is the rotation operator which shifts the momenta in the k_x and k_y as $2\pi/3$:

$$e^{i\,\frac{2\pi}{3}L_z}\,\vec{k}\,e^{-i\,\frac{2\pi}{3}L_z} = R\vec{k} \;\rightarrow\; e^{i\,\frac{2\pi}{3}L_z}\tilde{H}_0(\vec{k})e^{-i\,\frac{2\pi}{3}L_z} = \tilde{H}_0(R\vec{k}) \tag{D.2}$$

We must rewrite the Weyl Hamiltonian $H(k_x,k_y,k_z)$, given in Equation 3.5, with $H(k_x,\tilde{k}_y,k_z)$, where $\tilde{k}_y = k_y - \frac{2\pi}{\sqrt{3}}$. The k_z terms will not be considered because they are invariant under any rotation along the $\hat{z}$ axis:

$$\begin{aligned}\tilde{H}_0(k_x,\tilde{k}_y) = {} & 2t\cos(q)\left(\sin(k_x) - 2\sin\left(\frac{k_x}{2}\right)\cos\left(\frac{\sqrt{3}}{2}\tilde{k}_y\right)\right)\sigma_0 \\ & +2t\sin(q)\left(\cos(k_x) - \cos\left(\frac{1}{2}k_x\right)\cos\left(\frac{\sqrt{3}}{2}\tilde{k}_y\right)\right)\sigma_x \\ & +2t\sin(q)\left(\sin\left(\frac{1}{2}k_x\right)\sin\left(\frac{\sqrt{3}}{2}\tilde{k}_y\right)\right)\sigma_y\end{aligned} \tag{D.3}$$

The tunneling operators given in Equation 3.4 are:

$$U_1 = i\,e^{iq\sigma_x} \tag{D.4}$$

$$U_2 = i\,e^{iq\left(\frac{1}{2}\sigma_x + \frac{\sqrt{3}}{2}\sigma_y\right)} \tag{D.5}$$

$$U_3 = i\,e^{iq\left(\frac{1}{2}\sigma_x - \frac{\sqrt{3}}{2}\sigma_y\right)} \tag{D.6}$$

$$U_4 = i\,e^{iq\sigma_z} \tag{D.7}$$

If we look at Figure 3 the system has a $\frac{2\pi}{\sqrt{3}}$ translation in the k_y direction and it corresponds to sign change of U_2 and U_3:

$$\tilde{H}_0(k_x,\tilde{k}_y) = -t\,U_1 e^{i\,k_x} + t\,U_2 e^{i\,\frac{1}{2}k_x + \frac{\sqrt{3}}{2}\tilde{k}_y} + t\,U_3 e^{i\,\frac{1}{2}k_x - \frac{\sqrt{3}}{2}\tilde{k}_y} + h.c. \tag{D.8}$$

With the counterclockwise $2\pi/3$ rotation of the momenta:

$$\tilde{H}_0(R\vec{k}) = -t\,U_1 e^{-\frac{1}{2}\,i\,k_x + \frac{\sqrt{3}}{2}\,i\,\tilde{k}_y} + t\,U_2 e^{-i\,k_x} + t\,U_3 e^{i\,\frac{1}{2}k_x + \frac{\sqrt{3}}{2}\tilde{k}_y} + h.c. \tag{D.9}$$

The C_3 rotation operator is defined as:

$$C_3 = e^{i\,\frac{\pi}{3}\sigma_z} = \frac{1}{2}\sigma_0 + \frac{\sqrt{3}}{2}\,i\,\sigma_z \tag{D.10}$$

If the following equalities are fulfilled the system has C_3 rotational symmetry:

$$C_3^{\dagger}U_1C_3 = -U_3^{\dagger} \tag{D.11}$$

$$C_3^{\dagger}U_2C_3 = -U_1^{\dagger} \tag{D.12}$$

$$C_3^{\dagger}U_3C_3 = U_2 \tag{D.13}$$

I calculate the equalities:

$$C_3^{\dagger}U_1C_3 = i\,cos(q)\sigma_0 + sin(q)\left(\frac{1}{2}\sigma_x - \frac{\sqrt{3}}{2}\sigma_y\right) = -U_3^{\dagger} \tag{D.14}$$

$$C_3^{\dagger}U_2C_3 = i\,cos(q)\sigma_0 + sin(q)\sigma_x = -U_1^{\dagger} \tag{D.15}$$

$$C_3^{\dagger}U_3C_3 = i\,cos(q)\sigma_0 + sin(q)\left(-\frac{1}{2}\sigma_x - \frac{\sqrt{3}}{2}\sigma_y\right) = i\,e^{iq\left(\frac{1}{2}\sigma_x + \frac{\sqrt{3}}{2}\sigma_y\right)} = U_2 \tag{D.16}$$

E Calculation of the particle-hole symmetry

The canonical way of defining particle hole symmetry is

$$CH^*(-\vec{k})C^\dagger = -H(\vec{k}) \tag{E.1}$$

where $H(\vec{k})$ is the Weyl Hamiltonian shown in Equation 3.5 and C is a suitable matrix that we have to find.
The Weyl Hamiltonian in Equation 3.5 (with a negative sign) is given as:

$$\begin{aligned} -H(\vec{k}) = &-2\,t\,\cos(q)\left(\sin(k_x)+2\,\sin\left(\frac{1}{2}k_x\right)\cos\left(\frac{\sqrt{3}}{2}k_y\right)+\sin(k_z)\right)\sigma_0 - 2\,t\,\sin(q)\left(\cos(k_x)+\cos\left(\frac{1}{2}k_x\right)\cos\left(\frac{\sqrt{3}}{2}k_y\right)\right)\sigma_x \\ &+2\,t\,\sin(q)\left(\sin\left(\frac{1}{2}k_x\right)\sin\left(\frac{\sqrt{3}}{2}k_y\right)\right)\sigma_y - 2\,t\,\sin(q)\,\cos(k_z)\sigma_z \end{aligned} \tag{E.2}$$

The complex conjugated Weyl Hamiltonian with negative $\vec{k}$ is given as:

$$\begin{aligned} H^*(-\vec{k}) = &-2\,t\,\cos(q)\left(\sin(k_x)+2\,\sin\left(\frac{1}{2}k_x\right)\cos\left(\frac{\sqrt{3}}{2}k_y\right)+\sin(k_z)\right)\sigma_0 + 2\,t\,\sin(q)\left(\cos(k_x)+\cos\left(\frac{1}{2}k_x\right)\cos\left(\frac{\sqrt{3}}{2}k_y\right)\right)\sigma_x \\ &+2\,t\,\sin(q)\left(\sin\left(\frac{1}{2}k_x\right)\sin\left(\frac{\sqrt{3}}{2}k_y\right)\right)\sigma_y + 2\,t\,\sin(q)\,\cos(k_z)\sigma_z \end{aligned} \tag{E.3}$$

The unitary operators C must be defined so Equation E.1 is fulfilled and therefore the operators must show following properties:

$$\sigma_0 \to \sigma_0 \tag{E.4}$$

$$\sigma_x \to -\sigma_x \tag{E.5}$$

$$\sigma_y \to \sigma_y \tag{E.6}$$

$$\sigma_z \to -\sigma_z \tag{E.7}$$

Therefore the operator C, which has the properties shown in Equation E.4-E.7, is the Pauli matrix σ_y given as:

$$C = \begin{bmatrix} 0 & -i \\ i & 0 \end{bmatrix} = \sigma_y \tag{E.8}$$

With the Pauli matrix σ_y Equation E.1 is reduced to:

$$\sigma_y H^*(-\overrightarrow{k})\sigma_y = -H(\overrightarrow{k}) \tag{E.9}$$